Rare Met. (2020) 39(6):725–732
https://doi.org/10.1007/s12598-018-1190-z

RARE METALS
www.editorialmanager.com/rmet

Mechanical properties and thermal stability of 7055 Al alloy by minor Sc addition

Chong-Yu Liu, Guang-Biao Teng, Zong-Yi Ma*, Li-Li Wei, Wen-Biao Zhou, Hong-Feng Huang, Hai-Quan Qi

Received: 13 November 2017 / Revised: 15 December 2017 / Accepted: 22 November 2018 / Published online: 2 January 2019

Abstract This study investigated the effect of 0.25 wt% Sc addition on the microstructure and mechanical properties of AA 7055 alloy. The addition of Sc obviously refined the grains of AA 7055 alloy during casting, homogenizing, rolling, solution, and aging treatments due to the formation of primary and precipitate $Al_3(Sc,Zr)$ phase. The recrystallization and precipitation of AA 7055 alloy were inhibited during heat treatments by Sc addition. The Sc-containing AA 7055 alloy exhibited higher thermal stability than AA 7055 alloy during homogenizing treatment, because of the grain boundary pinning effect of nano-sized $Al_3(Sc,Zr)$ particles. Given its structure characteristics such as fine grains, fine η′ phase, and less η phase, AA 7055 alloy with added Sc showed good mechanical properties after aging at 120 °C for 24 h, with an ultimate tensile strength (UTS) of 679 MPa and elongation (EL) of 14%. This work provides an effective strategy to fabricate Al–Zn–Mg(–Cu) series (7xxx) alloys with excellent mechanical properties.

Keywords Al alloy; Sc addition; Microstructure; Mechanical properties

C.-Y. Liu, G.-B. Teng, L.-L. Wei, H.-F. Huang, H.-Q. Qi
Key Laboratory of New Processing Technology for Nonferrous Metal and Materials, Ministry of Education, Guilin University of Technology, Guilin 541004, China

C.-Y. Liu, Z.-Y. Ma*
Shenyang National Laboratory for Materials Science, Institute of Metal Research, Chinese Academy of Sciences, Shenyang 110016, China
e-mail: zyma@imr.ac.cn

W.-B. Zhou
Alnan Aluminium Co., Ltd, Nanning 530000, China

1 Introduction

Al–Zn–Mg(–Cu) series (7xxx) alloys are widely used in aircraft manufacturing industry because of their low density and excellent mechanical properties [1–3]. Compared with other 7xxx alloys, AA 7055 alloy with high Zn, Cu and Zr contents exhibited higher strength and high ductility [4]. Further improvement in the mechanical properties of AA 7055 alloy is desirable to extend the engineering application of commercial Al alloys. The addition of Zr and rare-earth Sc into commercial Al alloys has been proven to be an effective approach in improving their mechanical properties [5–7]. The primary and precipitated Al_3Sc or $Al_3(Sc,Zr)$ phases can lead to the grain refinement of Al alloys during solidification, heat treatments and deformations, thereby promoting grain boundary (GB) strengthening of Al alloys [8–13]. Recently, Chen et al. [14, 15] and Jiang et al. [16, 17] found that the segregation of Sc atoms at the θ′/matrix interfaces in Al–Cu–Sc alloys can inhibit the growth of θ′ phase and the transformation of θ′ into θ phase, thereby increasing the precipitation strengthening of Al alloys.

Clearly, the addition of Sc and Zr to Al alloys is an effective method for improving their thermal stability and mechanical properties. However, the effects of Sc on the microstructure and mechanical properties of AA 7055 alloy, which were characterized by high Zn (> 7.6 wt%), Cu (> 2.0 wt%), and Zr (> 0.15 wt%) contents, high strength (ultimate tensile strength, UTS > 600 MPa), and good ductility (tensile elongation, EL > 10%), have rarely been reported.

In the present study, AA 7055 and AA 7055 containing 0.25 wt% Sc (AA 7055–0.25Sc) alloys were subjected to microstructural examinations, hardness measurements and tensile tests under casting, homogenizing, rolling, solution

and aging treatment conditions. The aim of this study is to understand the effects of minor Sc addition on the microstructure and mechanical properties of AA 7055 alloy during the above processes. This study can provide a basis for compositional design of high-performance 7xxx series Al alloys.

2 Experimental

AA 7055 and AA 7055–0.25Sc alloys were prepared by casting. The chemical compositions of those two alloys are shown in Table 1. The ingots were homogenized at 470 °C for 26 h and rapidly quenched to room temperature by immersing into water. After homogenization treatment, the ingots were hot rolled from 10 to 3 mm at 470 °C with seven rolling passes. Between every rolling pass, the samples were reheated in a furnace at the prescribed rolling temperatures for 3 min. The rolled samples were subsequently subjected to solution treatment at 470 °C for 2 h, water quenched (the samples were defined as SS), and then aged at 120 °C for different durations from 1 to 72 h.

The microstructures of the alloys were examined by optical microscope (OM, Leica-DMi8) and transmission electron microscope (TEM, JEM-2010). The films for TEM were prepared by grinding to a thickness of 50 μm, followed by thinning using a twinjet electropolishing device. The OM and TEM specimens were prepared in the rolling direction–normal direction of samples. Hardness measurement was performed with a Vickers microhardness tester. The tensile tests were conducted on an Instron-3369-type testing machine at a strain rate of 4×10^{-4} s^{-1} according to the ISO 6892-1:2009. The tensile specimen was machined parallel to the rolling direction. The fracture surfaces following the tensile tests were observed by scanning electron microscope (SEM, S-4800).

3 Results and discussion

Figure 1 shows OM images of AA 7055 and AA 7055–0.25Sc alloys in their casting and homogenizing treatment states. The as-cast AA 7055 alloy was characterized by a typical dendritic structure (Fig. 1a). The addition of 0.25 wt% Sc into AA 7055 alloy led to the formation of refined and equiaxed grains (Fig. 1b). A large number of previous studies confirmed that the primary Al_3(Sc,Zr) phase can serve as a heterogeneous nucleation site for Al grains during solidification and resulted in the formation of equiaxed Al grains and grain refinement [9]. Thus, the grain size of AA 7055–0.25Sc alloy was smaller than that of AA 7055 alloy in their casting states. After homogenization treatment, the dendritic grains changed into equiaxed grains, and some of them reached as large as 1000 μm in the AA 7055 alloy (Fig. 1c). By comparison, the grain size or structure of the AA 7055–0.25Sc alloy did not significantly change after homogenization treatment, and the average grain size of this sample was ~ 60 μm (Fig. 1d).

Table 1 Chemical composition of AA 7055 and AA 7055–0.25Sc alloys (wt%)

Alloys	Zn	Mg	Cu	Zr	Sc
AA 7055	7.82	1.95	2.24	0.16	–
AA 7055–0.25Sc	7.81	1.93	2.24	0.16	0.25

Figure 2 shows TEM images of AA 7055 and AA 7055–0.25Sc alloys after homogenizing treatment. The equiaxed particles with sizes of 20–30 nm were observed in the AA 7055 alloy (Fig. 2a). According to the chemical composition and heat treatment, those particles should be Al_3Zr phase. By comparison, much higher density of nano-sized particles was observed in the AA 7055–0.25Sc alloy than in AA 7055 alloy. The selected area diffraction revealed that the nano-sized particles were Al_3(Sc,Zr) phase (Fig. 2b). Compared with AA 7055 alloy, AA 7055–0.25Sc alloy showed significantly higher thermal stability during homogenizing treatment, and the average grain size of AA 7055–0.25Sc alloys was one order of magnitude lower than that of AA 7055 alloy after homogenization (Fig. 1c, d). This phenomenon is attributed to high density of nano-sized Al_3(Sc,Zr) particles precipitated from Al lattice, which can strongly pin grain boundaries (GBs) during heat treatment [18, 19] and thereby prevent an intense grain growth in the AA 7055–0.25Sc alloy.

Figure 3 shows OM images of the rolled AA 7055 and AA 7055–0.25Sc samples. Both samples exhibited elongated grains in the rolling direction. The average short dimension sizes of the grains in the as-rolled AA 7055 and AA 7055–0.25Sc alloys were estimated to be ~ 30 μm (Fig. 3a) and ~ 7 μm (Fig. 3b), respectively. Smaller grain size of AA 7055–0.25Sc alloy than that of AA 7055 alloy after the same rolling is attributed to the following factors. First, the AA 7055–0.25Sc alloy had smaller grain size than the AA 7055 alloy prior to rolling. Second, the nano-sized Al_3(Sc,Zr) particles precipitated in the AA 7055–0.25Sc alloy during homogenizing treatment (Fig. 2b) strongly pinned the GBs during the rolling, inhibiting both recovery and recrystallization, and therefore, the deformed structures were retained [18, 20].

Figure 4 shows the age-hardening curves of AA 7055 and AA 7055–0.25Sc alloys during aging at 120 °C. Those two alloys exhibited obvious age-hardening behavior, and

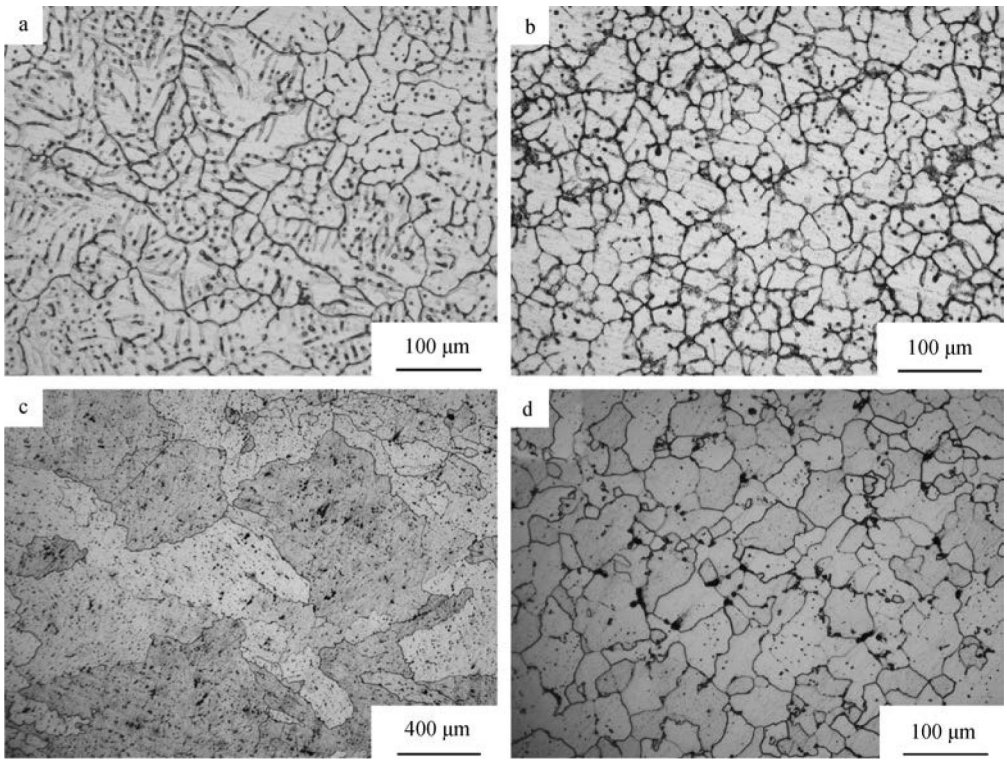

Fig. 1 OM images of **a** as-cast and **c** homogenization-treated AA 7055 alloy and **b** as-cast and **d** homogenization-treated AA 7055–0.25Sc alloy

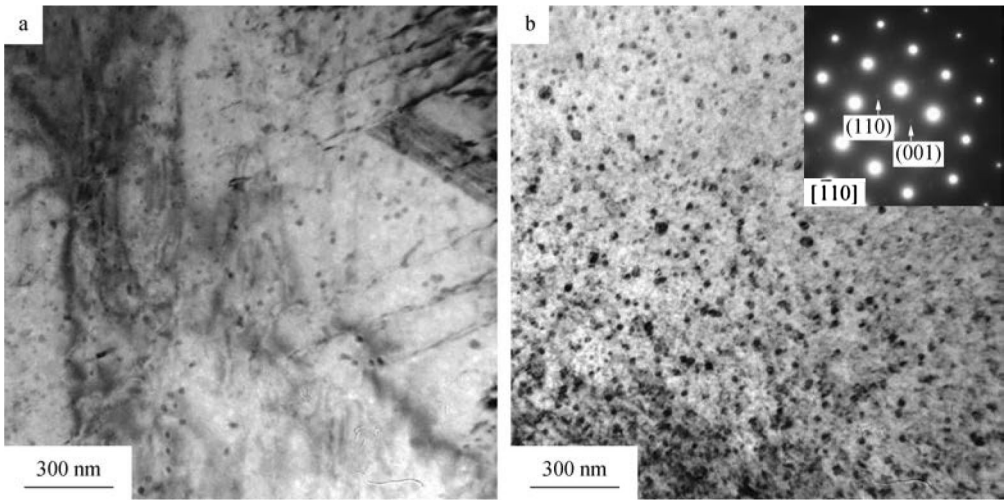

Fig. 2 TEM images of **a** AA 7055 and **b** AA 7055–0.25Sc alloys after homogenizing treatment

their peak-aging (PA) times were 24–26 h. The hardness value of AA 7055–0.25Sc alloy was always higher than that of the AA 7055 alloy within the entire aging period of up to 72 h.

Figure 5 shows OM images of the peak-aged AA 7055 and AA 7055–0.25Sc alloys. From Fig. 5a, it can be seen that partial recrystallization occurred in the AA 7055 alloy. However, for AA 7055–0.25Sc alloy, no recrystallization grains were observed, and the fibrous rolling deformation organization was well preserved after solution and aging treatments (Fig. 5b). Figure 6 shows TEM images of AA 7055 and AA 7055–0.25Sc alloys after aging at 120 °C for 12 h (under-aged condition). For AA 7055 alloy, the high density of η' precipitates with less than 3 nm in size was observed in the grain interior, and the η precipitates with large size (larger than 50 nm) were discontinuously distributed along the GBs (Fig. 6a, b). By comparison, more subgrain boundaries were obtained in AA 7055–0.25Sc

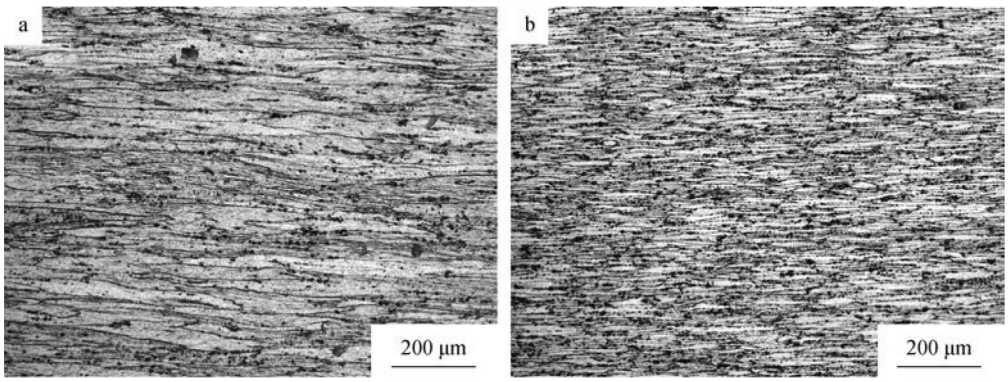

Fig. 3 OM images of as-rolled **a** AA 7055 and **b** AA 7055–0.25Sc alloys

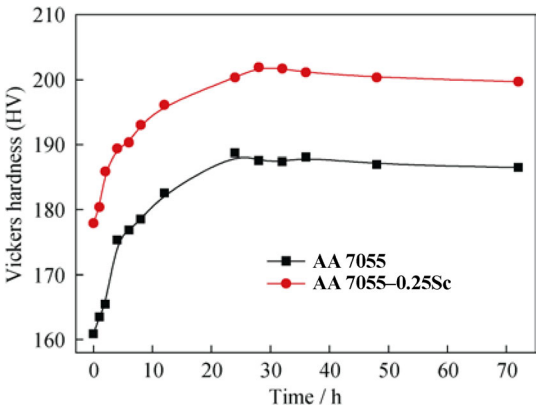

Fig. 4 Variation of Vickers hardness with aging time at 120 °C for AA 7055 and AA 7055–0.25Sc alloys

alloy (Fig. 6c), and high density of fisheye-like $Al_3(Sc,Zr)$ particles were observed in AA 7055–0.25Sc alloy, with some of them located at GBs (Fig. 6d).

Figure 7 shows TEM images of AA 7055 and AA 7055–0.25Sc alloys after aging at 120 °C for 24 h (PA). For AA 7055 alloy, the precipitated phase coarsened, and some of them reached as large as ~ 60 nm (Fig. 7a). Furthermore, the precipitate free zones (PFZ) were observed (Fig. 7b). The coarsening of precipitates was inhibited in AA 7055–0.25Sc alloy during further aging (Fig. 7c), and the magnified micrograph showed that the η precipitates were also discontinuously distributed along the GBs, but their density was lower than that in AA 7055 alloy (Fig. 7b, d). $Al_3(Sc,Zr)$ particles were also observed in the grain interior defect, such as at dislocations (Fig. 7d), and no obvious PFZ was observed in this alloy after aging, as shown by the inset in Fig. 7d. Clearly, the recrystallization of AA 7055 alloy during solution and aging treatments were influenced by the minor Sc addition. Numerous $Al_3(Sc,Zr)$ particles located at the GBs in AA 7055–0.25Sc alloys (Figs. 6d, 7d) can strongly pin GBs during heat treatments [19], thereby inhibiting recrystallization and preventing intense grain growth (Fig. 5). Thus, the fine microstructure with fibrous shape grains was well preserved in AA 7055–0.25Sc alloy after heat treatments.

The precipitation behavior of AA 7055 alloys during solution and aging treatments was inhibited by minor Sc addition (Figs. 6, 7). A similar phenomenon was also observed in other Sc-containing 7xxx alloys [9, 21]. Using three-dimensional atom probe, Chen et al. [14] and Jiang et al. [17] found the segregation of Sc atoms at the precipitated metastable phase/Al matrix interfaces in Al–Cu–Sc alloys, and the growth of metastable phase and

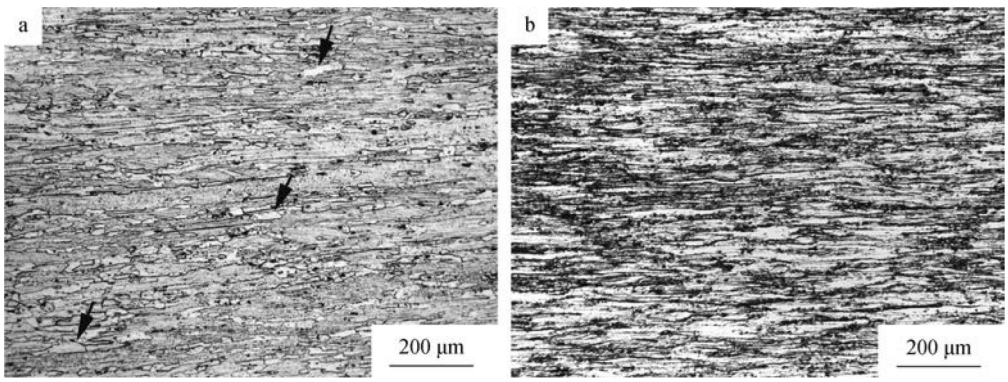

Fig. 5 OM images of **a** AA 7055 and **b** AA 7055–0.25Sc alloys after aging at 120 °C for 24 h (PA) (arrows in **a** denoting recrystallized grains)

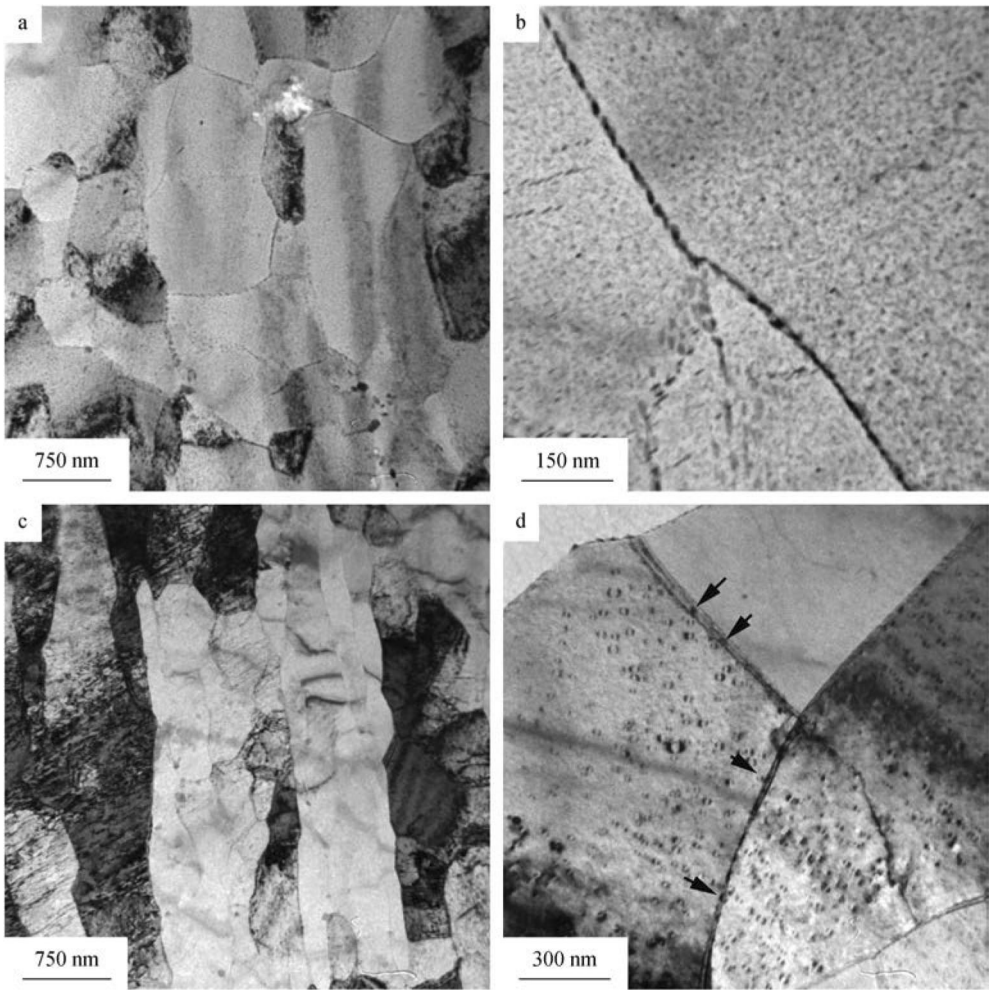

Fig. 6 TEM images of **a, b** AA 7055 and **c, d** AA 7055–0.25Sc alloys after aging at 120 °C for 12 h (arrows in **d** denoting $Al_3(Sc,Zr)$ phase)

transformation of metastable into stable phase were inhibited by those Sc atoms [14]. In the present study, large numbers of Sc atoms may also locate at the metastable η′ phase/Al matrix interfaces. Thus, η′ phase exhibited high thermal stability during aging treatment.

The GBs and quenching-induced crystal defects, such as vacancies and dislocations, provided preferential nucleation sites for precipitates during artificial aging [22]. For 7xxx alloys, the quenching-induced crystal defects would be annihilated during aging, and only the GBs provided heterogeneous nucleation sites for the precipitates. During aging, the dislocations near GBs would be aggregated around GBs, and this condition was beneficial to the solute element diffusion to GBs; then, the metastable precipitates at GBs grew continuously and transformed into stable phase [23–25]. Thus, large η precipitates along GBs and PFZ were obtained in AA 7055 alloys (Fig. 7b).

High density of nano-sized $Al_3(Sc,Zr)$ particles was obtained in AA 7055–0.25Sc alloys after homogenizing treatment (Fig. 2b), and $Al_3(Sc,Zr)$ particles can effectively pin dislocations during heat treatments or deformations [26–28]. Thus, the movements and annihilations of quenching-induced dislocations were suppressed during aging due to the pinning effect of $Al_3(Sc,Zr)$ particles (Fig. 7d), and the nucleation sites for precipitates provided for AA 7055–0.25Sc alloy increased. Thus, the density of η phase along GBs in AA 7055–0.25Sc alloy was lower than that in AA 7055 alloy (Fig. 7b, d).

The stress–strain curves of AA 7055 and AA 7055–0.25Sc alloys are compared in Fig. 8. The mechanical properties of the two alloys are given in Table 2. Both the strength and EL of the two alloys increased with aging time increasing. AA 7055–0.25Sc alloy exhibited higher strength and ductility than AA 7055 alloys under the same treatment condition. AA 7055–0.25Sc alloy after aging at 120 °C for 24 h showed the best mechanical properties, and the UTS and EL of this sample reached up to 679 MPa and 14%, respectively.

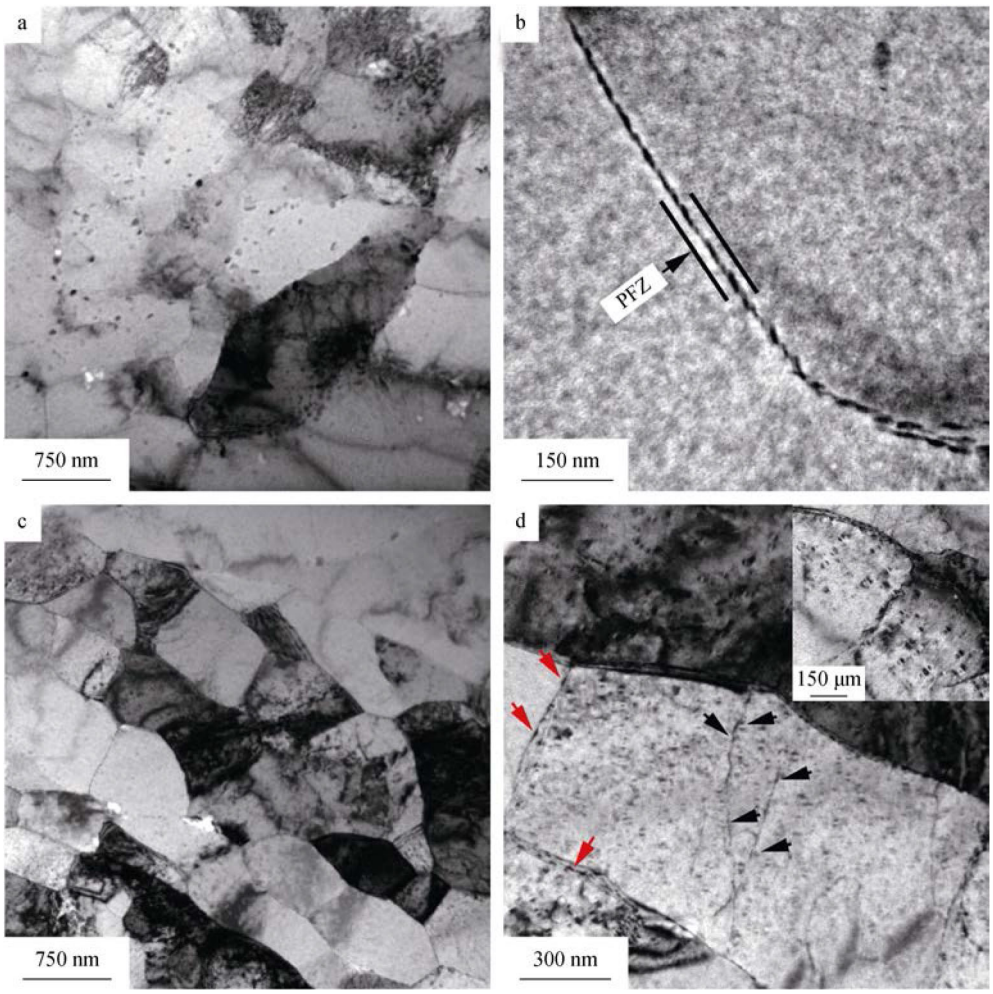

Fig. 7 TEM images of **a, b** AA 7055 and **c, d** AA 7055–0.25Sc alloys after aging at 120 °C for 24 h (red and black arrows in panel **d** denoting η and Al_3(Sc,Zr) phases, respectively)

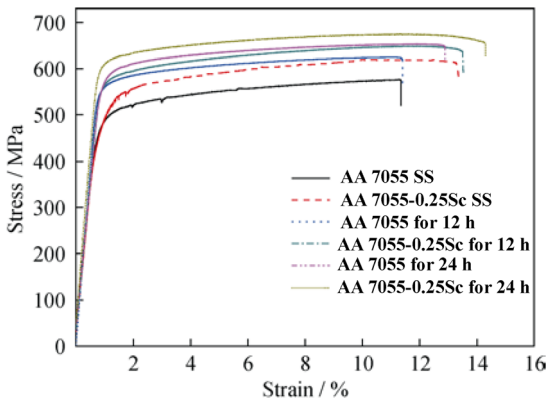

Fig. 8 Stress–strain curves of AA 7055 and AA 7055–0.25Sc alloys after solid solution and aging at 120 °C

Table 2 Tensile properties of AA 7055 and AA 7055–0.25Sc alloys with various aging parameters

Alloys	Yield strength (YS)/MPa	UTS/MPa	EL/%
SS			
AA 7055	467	576	11
AA 7055–0.25Sc	470	620	13
120 °C/12 h			
AA 7055	562	620	11
AA 7055–0.25Sc	567	649	14
120 °C/24 h			
AA 7055	577	654	13
AA 7055–0.25Sc	600	679	14

Compared with AA 7055 alloys, AA 7055–0.25Sc alloys exhibited higher strength mainly due to the increased GB and precipitation strengthenings, which were caused by the fine grains (Fig. 5), fine η′ and less η phases (Figs. 6, 7). The fracture surfaces of AA 7055 and AA 7055–0.25Sc alloys after aging at 120 °C for 24 h are shown in Fig. 9. Compared with those of AA 7055 alloy, the fracture surfaces of AA 7055–0.25Sc alloy exhibited fine and

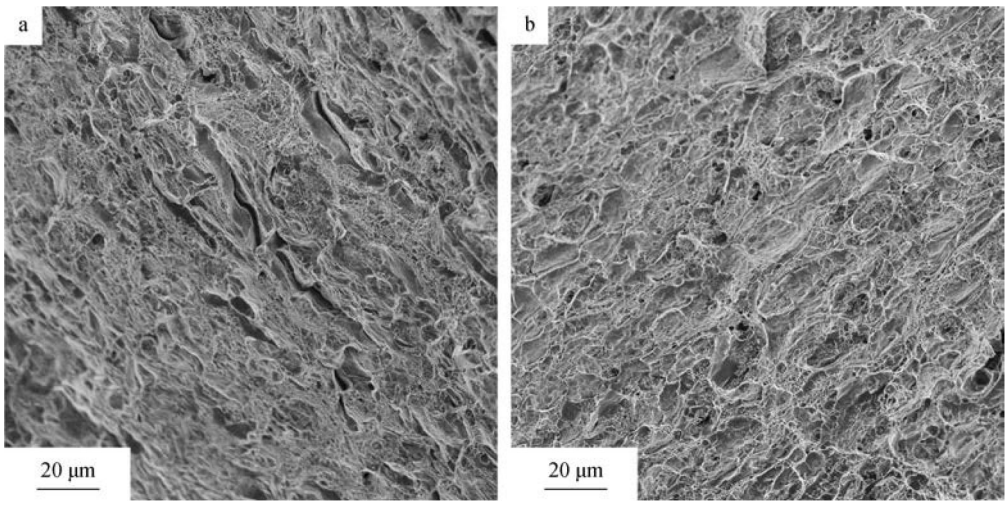

Fig. 9 Fracture surfaces of **a** AA 7055 and **b** AA 7055–0.25Sc alloys after aging at 120 °C for 24 h

homogenous dimples due to the fine and homogenous grains of this sample. This structure characteristics of AA 7055–0.25Sc alloy showed that the strain localization can be prevented by redistribution of the stresses during tension, thereby achieving considerable elongation before failure. Thus, AA 7055–0.25Sc alloy exhibited high ductility.

Figure 10 shows tensile properties of 7xxx alloys with Sc additions from the present study and previous reports. The data of AA 7055–0.25Sc alloy were presented above the shade, indicating that this sample owned balanced mechanical properties. The UTS of 7xxx-Sc alloys increased with Zn content increasing. Thus, the UTS of the present AA 7055–0.25Sc alloy is lower than that of Al–8.82Zn–2.08Mg–0.8Cu–0.31Sc–0.3Zr alloy [5] but higher than those of other alloys. Compared with 7xxx-Sc alloys in the previous studies [5, 6, 9, 10, 29], the present AA 7055–0.25Sc alloy exhibited higher EL. Zhang et al. [5] claimed that the low EL in 7xxx-Sc alloys with high strength was always due to the high density of η phase in GBs. In the present study, AA 7055–0.25Sc alloy exhibited low density of η phase in GBs (Fig. 7d). Thus, the ductility of this sample was improved. Furthermore, AA 7055–0.25Sc alloy showed finer grains and lower Mn, Si, and Fe contents than 7xxx-Sc alloys in the previous studies [6, 9, 10, 29]. Therefore, the crack growth resistance of the AA 7055–0.25Sc alloy can be improved during tensile test [30], which is also beneficial to the improvement in EL.

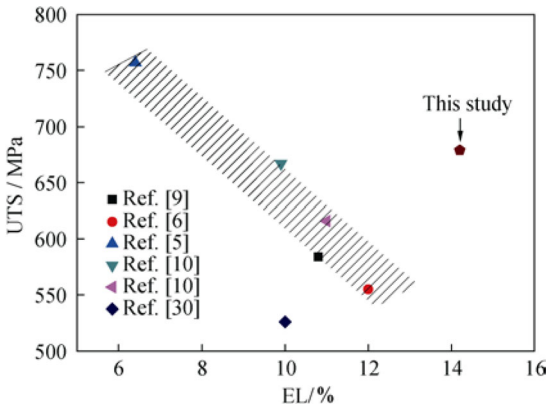

Fig. 10 Summary tensile properties of 7xxx-Sc alloys from previous studies (Ref. [9]: Al–5.42Zn–1.98Mg–0.24Sc–0.12Zr; Ref. [6]: Al–5.7Zn–1.98Mg–0.33Cu–0.25Sc–0.1Zr; Ref. [5]: Al–8.82Zn–2.08Mg–0.8Cu–0.31Sc–0.3Zr; Ref. [10]: Al–7.11Zn–2.49Mg–0.22Cu–0.22Sc–0.4Zr, Al–6.84Zn–2.6Mg–0.21Cu–0.37Sc–0.18Zr; Ref. [30]: Al–5.5Zn–2Mg–0.2Sc–0.1Zr) and AA 7055–0.25Sc alloy with PA condition in this study

4 Conclusion

In this study, the potential to achieve high mechanical properties and good thermal stability in AA 7055 alloys via Sc addition was demonstrated. The addition of 0.25 wt% Sc into AA 7055 alloy led to the formation of refined and equiaxed-casting grains because primary $Al_3(Sc,Zr)$ phase can promote the heterogeneous nucleation during solidification. The Sc addition considerably improved the thermal stability of the AA 7055 alloy during homogenizing treatment due to the GB pinning effect by the precipitated $Al_3(Sc,Zr)$ phase. The average grain size of the as-rolled AA 7055–0.25Sc alloy was ~ 7 μm, which was significantly lower than that of the as-rolled AA 7055 alloy under the same rolling. The recrystallization and precipitation behavior of AA 7055–0.25Sc alloy were inhibited during the subsequent solution and aging due to the effects of nano-sized $Al_3(Sc,Zr)$ phase and Sc atoms. AA 7055–0.25Sc alloy exhibited higher strength and ductility than AA 7055 alloy under the same heat treatment due to

the fine grains, fine η′ phase and less η phase in AA 7055–0.25Sc alloy. Compared with previous 7xxx-Sc alloys, the present AA 7055–0.25Sc alloy with the peak-aging condition exhibited balanced mechanical properties.

Acknowledgements This work was financially supported by the National Natural Science Foundation of China (No. 51601045), the Research Program of Science and Technology of Guangxi (No. GKAB16380021) and the Guangxi "Bagui" Teams for Innovation and Research.

References

[1] Wei LL, Pan QL, Huang HF, Feng L, Wang YL. Influence of grain structure and crystallographic orientation on fatigue crack propagation behavior of 7050 alloy thick plate. Int J Fatigue. 2014;66(9):55.
[2] Zuo JR, Hou LG, Shi JT, Cui H, Zhuang LZ, Zhang JS. Enhanced plasticity and corrosion resistance of high strength Al–Zn–Mg–Cu alloy processed by an improved thermomechanical processing. J Alloys Compd. 2017;716(9):220.
[3] Wei LL, Pan QL, Wang YL, Feng L, Huang HF. Characterization of fracture and fatigue behavior of 7050 aluminum alloy ultra-thick plate. J Mater Eng Perform. 2013;22(9):2665.
[4] Liu SD, Zhang XM, Chen MA, You JH. Influence of aging on quench sensitivity effect of 7055 aluminum alloy. Mater Charact. 2008;59(1):53.
[5] Zhang M, Liu T, He CN, Ding J, Liu EZ, Shi CS, Li JJ, Zhao NQ. Evolution of microstructure and properties of Al–Zn–Mg–Cu–Sc–Zr alloy during aging treatment. J Alloys Compd. 2016;658(2):946.
[6] Deng Y, Yin ZM, Duan JQ, Zhao K, Tang B, He ZB. Evolution of microstructure and properties in a new type 2 mm Al–Zn–Mg–Sc–Zr alloy sheet. J Alloys Compd. 2012;517(2):118.
[7] Huang HF, Jiang F, Zhou J, Wei LL, Zhong MC, Liu XT. Hot deformation behavior and microstructural evolution of as-homogenized Al–6Mg–0.4Mn–0.25Sc–0.1Zr alloy during compression at elevated temperature. J Alloys Compd. 2015;644(9):862.
[8] Zhou WB, Liu CY, Yu PF, Zhang B, Ma ZY, Luo K, Ma MZ, Liu RP. Effect of scandium on microstructure and mechanical properties of high zinc concentration aluminum alloys. Mater Charact. 2017;127(5):371.
[9] Li B, Pan QL, Huang X, Yin ZM. Microstructures and properties of Al–Zn–Mg–Mn alloy with trace amounts of Sc and Zr. Mater Sci Eng A. 2014;616(10):219.
[10] Li G, Zhao NQ, Liu T, Li JJ, He CN, Shi CS, Liu EZ, Sha JW. Effect of Sc/Zr ratio on the microstructure and mechanical properties of new type of Al–Zn–Mg–Sc–Zr alloys. Mater Sci Eng A. 2014;617(11):219.
[11] Chen Y, Liu CY, Zhang B, Ma ZY, Zhou WB, Jiang HJ, Huang HF, Wei LL. Effects of friction stir processing and minor Sc addition on the microstructure, mechanical properties, and damping capacity of 7055 Al alloy. Mater Charact. 2018;135(1):25.
[12] Chanyathunyaroj K, Patakham U, Kou S, Limmaneevichit C. Mechanical properties of squeeze-cast Al–7Si–0.3Mg alloys with Sc-modified Fe-rich intermetallic compounds. Rare Met. 2018;37(9):769.
[13] Sun SP, Li XP, Yang J, Wang HJ, Jiang Y, Yi DQ. Point defect concentrations of $L1_2$-Al_3X(Sc, Zr, Er). Rare Met. 2018;37(8):699.
[14] Chen BA, Liu G, Wang RH, Zhang JY, Jiang L, Song JJ, Sun J. Effect of interfacial solute segregation on ductile fracture of Al–Cu–Sc alloys. Acta Mater. 2013;61(5):1676.
[15] Chen BA, Pan L, Wang RH, Liu G, Cheng PM, Xiao L, Sun J. Effect of solution treatment on precipitation behaviors and age hardening response of Al–Cu alloys with Sc addition. Mater Sci Eng A. 2011;530(12):607.
[16] Jiang L, Li JK, Cheng PM, Liu G, Wang RH, Chen BA, Zhang JY, Sun J, Yang MX, Yang G. Experiment and modeling of ultrafast precipitation in an ultrafine-grained Al–Cu–Sc alloy. Mater Sci Eng A. 2014;607(6):596.
[17] Jiang L, Li JK, Liu G, Wang RH, Chen BA, Zhang JY, Sun J, Yang MX, Yang G, Yang J, Cao XZ. Length-scale dependent microalloying effects on precipitation behaviors and mechanical properties of Al–Cu alloys with minor Sc addition. Mater Sci Eng A. 2015;637(6):139.
[18] Deng Y, Xu GF, Yin ZM, Lei XF, Huang JW. Effects of Sc and Zr microalloying additions on the recrystallization texture and mechanism of Al–Zn–Mg alloys. J Alloys Compd. 2013;580(12):412.
[19] Avtokratova E, Sitdikov O, Markushev M, Mulyukov R. Extraordinary high-strain rate superplasticity of severely deformed Al–Mg–Sc–Zr alloy. Mater Sci Eng A. 2012;538(10):386.
[20] Deng Y, Yin ZM, Zhao K, Duan JQ, He ZB. Effects of Sc and Zr microalloying additions on the microstructure and mechanical properties of new Al–Zn–Mg alloys. J Alloys Compd. 2012;530(7):71.
[21] Wu LM, Seyring M, Rettenmayr M, Wang WH. Characterization of precipitate evolution in an artificially aged Al–Zn–Mg–Sc–Zr alloy. Mater Sci Eng A. 2010;527(4–5):1068.
[22] Liu CY, Qu B, Ma ZY, Ma MZ, Liu RP. Recrystallization, precipitation, and resultant mechanical properties of rolled Al–Zn alloy after aging. Mater Sci Eng A. 2016;657(3):284.
[23] Wang D, Ni DR, Ma ZY. Effect of pre-strain and two-step aging on microstructure and stress corrosion cracking of 7050 alloy. Mater Sci Eng A. 2008;494(1–2):360.
[24] Wang D, Ma ZY, Gao ZM. Effects of severe cold rolling on tensile properties and stress corrosion cracking of 7050 aluminum alloy. Mater Chem Phys. 2009;117(1):228.
[25] Wang D, Ma ZY. Effect of pre-strain on microstructure and stress corrosion cracking of over-aged 7050 aluminum alloy. J Alloys Compd. 2009;469(1–2):445.
[26] Deng Y, Peng B, Xu GF, Pan QL, Yin ZM, Ye R, Wang YJ, Lu LY. Effects of Sc and Zr on mechanical property and microstructure of tungsten inert gas and friction stir welded aerospace high strength Al–Zn–Mg alloys. Mater Sci Eng A. 2015;639(7):500.
[27] Lefebvre W, Danoix F, Hallem H, Forbord B, Bostel A, Marthinsen K. Precipitation kinetic of Al_3(Sc, Zr) dispersoids in aluminium. J Alloy Compd. 2009;470(1–2):107.
[28] Knipling KE, Karnesky RA, Lee CP, Dunand DC, Seidman DN. Precipitation evolution in Al–0.1Sc, Al–0.1Zr and Al–0.1Sc–0.1Zr (at%) alloys during isochronal aging. Acta Mater. 2010;58(15):5184.
[29] He ZB, Yin ZM, Lin S, Deng Y, Shang BC, Zhou X. Preparation, microstructure and properties of Al–Zn–Mg–Sc alloy tubes. J Rare Earths. 2010;28(4):641.
[30] Zuo JR, Hou LG, Shi JT, Cui H, Zhuang LZ, Zhang JS. Effect of deformation induced precipitation on grain refinement and improvement of mechanical properties AA 7055 aluminum alloy. Mater Charact. 2017;130(8):123.